Langmuir
Article
pubs.acs.org/Langmuir

Dilational Lateral Stress in Drying Latex Films

Alexander M. König,[†] Elodie Bourgeat-Lami,[‡] Véronique Mellon,[‡] Kerstin von der Ehe,[†] Alexander F. Routh,[§] and Diethelm Johannsmann*,[†]

[†]*Institute of Physical Chemistry, Clausthal University of Technology, Arnold-Sommerfeld-Str. 4, D-38678 Clausthal-Zellerfeld, Germany,* [‡]*Université de Lyon, Univ. Lyon 1, CPE Lyon, CNRS UMR 5265, Laboratoire de Chimie, Catalyse, Polymères et Procédés (C2P2), LCPP group, 43 Bd du 11 Novembre 1918, F-69616, Villeurbanne, France, and* [§]*Department of Chemical Engineering and Biotechnology, BP Institute, University of Cambridge, Madingley Road, Cambridge CB3 0EZ, U.K.*

Received January 6, 2009. Revised Manuscript Received January 20, 2010

Drying latex films usually experience tensile stress due to the reduction in volume. While an unconstrained film would shrink affinely in all three dimensions, a coating can only shrink along the vertical and therefore exerts tensile stress onto the substrate. Using an instrument capable of producing maps of the stress distribution, we found that *dilational stress* sometimes develops as well. The in-plane stress was monitored by spreading the latex dispersion on a flexible membrane. Usually, the membrane bends upward under the tensile stress exerted by the film, but it may also bend downward. Dilational stress was only found with samples showing a strong coffee stain effect, that is, samples in which there is a significant lateral flow from the center to the edge while the film dries. During drying, particles consolidate first at the edge because of the lower height in this region. Continued evaporation from the consolidated region results in a water flow toward the edge, exerting a force onto the latex particles. At the time, when the network is formed, any single sphere must be in a force-balance condition: the network must exert an elastic force onto the sphere which just compensates the viscous drag. Pictorially speaking, a spring (an elastic network) is created while an external force acts onto it. Once the flow stops, the drag force vanishes and the internal stress, which previously compensated the drag, expands the film laterally. This phenomenon can lead to buckling. Given that lateral flow of liquid while films dry is a rather common occurrence, this mode of structure formation should be widespread. It requires lateral flow in conjunction with elastic recovery of the particle network.

Introduction

The process of film formation from aqueous polymer dispersions (latexes) is of much practical relevance in the coatings industry because waterborne paints release little or no volatile organic compounds (VOCs) upon drying.[1−3] Environmental regulations have led to a steady increase in market volume of such coatings. Polymer dispersions offer numerous options to improve and adjust coating properties, which do not exist for conventional, solvent-based coatings. For instance, it is rather easy to produce nanostructured composites by employing either latex blends[4,5] or core−shell particles.[6] On the other hand, film formation poses challenges as well. During drying, the material experiences a sequence of transformations, involving water loss, particle deformation, and interparticle coalescence. Typical problems are skin formation,[7−10] the development of an "orange peel" like surface,[11] cracking,[12−14] and insufficient cohesion.[15]

Of particular importance in the context of the study reported here are stresses developing during shrinkage. Stress is the source of one of the classical failure modes of film formation, which is cracking. In many (but not all) cases, shrinkage would occur affinely (both in-plane and along the vertical) if there were no external constraints. The substrate imposes such constraints, producing a tensile in-plane stress. If the substrate is slightly flexible, it bends upward,[16] which is easily detected.

Tensile stress in drying films has been quantitatively determined by numerous researchers employing the beam bending technique.[17−19] While tensile lateral stress certainly is the rule, one also finds the opposite behavior. In some cases, the film laterally *expands*. The phenomenon usually is localized and transient. Since the classical beam bending instruments measure the average stress, they easily miss such phenomena. We have recently developed an instrument capable of determining spatially resolved maps of the stress distribution.[20] The measurement is based on the deformation of a flexible membrane (Figure 1A). Using automated image analysis, one generates a map of film stress as a function of location and time.

*Corresponding author. E-mail: johannsmann@pc.tu-clausthal.de.

(1) Keddie, J. L. *Mater. Sci. Eng., R* **1997**, *21*, 101.
(2) Steward, P. A.; Hearn, J.; Wilkinson, M. C. *Adv. Colloid Interface Sci.* **2000**, *86*, 195.
(3) Winnik, M. A. *Curr. Opin. Colloid Interface Sci.* **1997**, *2*, 192.
(4) Tzitzinou, A.; Keddie, J. L.; Geurts, J. M.; Peters, A.; Satguru, R. *Macromolecules* **2000**, *33*, 2695.
(5) Colombini, D.; Hassander, H.; Karlsson, O. J.; Maurer, F. H. J. *Macromolecules* **2004**, *37*, 6865.
(6) Juhue, D.; Lang, J. *Macromolecules* **1995**, *28*, 1306.
(7) Eckersley, S. T.; Rudin, A. *Prog. Org. Coat.* **1994**, *23*, 387.
(8) Routh, A. F.; Russel, W. B. *Ind. Eng. Chem. Res.* **2001**, *40*, 4302.
(9) Erkselius, S.; Wadso, L.; Karlsson, O. J. *J. Colloid Interface Sci.* **2008**, *317*, 83.
(10) Koenig, A. M.; Weerakkody, T. G.; Keddie, J. L.; Johannsmann, D. *Langmuir* **2008**, *24*, 7580.
(11) Abbasian, A.; Ghaffarian, S. R.; Mohammadi, N.; Khosroshahi, M. R.; Fathollahi, M. *Prog. Org. Coat.* **2004**, *49*, 229.
(12) Lee, W. P.; Routh, A. F. *Langmuir* **2004**, *20*, 9885.
(13) Russel, W. B.; Wu, N.; Man, W. *Langmuir* **2008**, *24*, 1721.
(14) Singh, K. B.; Tirumkudulu, M. S. *Phys. Rev. Lett.* **2007**, *98*, 218302.
(15) Voyutskii, S. S. *J. Polym. Sci.* **1958**, *32*, 528.
(16) Stoney, G. *Proc. R. Soc. London* **1909**, *A82*, 172.
(17) Francis, L. F.; McCormick, A. V.; Vaessen, D. M.; Payne, J. A. *J. Mater. Sci.* **2002**, *37*, 4897.
(18) Martinez, C. J.; Lewis, J. A. *Langmuir* **2002**, *18*, 4689.
(19) Petersen, C.; Heldmann, C.; Johannsmann, D. *Langmuir* **1999**, *15*, 7745.
(20) von der Ehe, K.; Johannsmann, D. *Rev. Sci. Instrum.* **2007**, *78*, 113904.

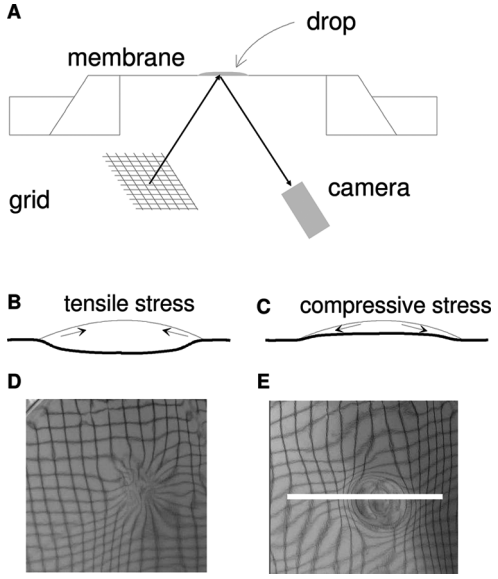

Figure 1. Sketch of the experimental setup for stress mapping (A). If the stress is of tensile nature, it bends the membrane upward (B). Otherwise, the membrane adopts a concave shape when observed from below (C). Panels D and E show photographs taken on samples that had been removed from the support. The mirror is convex in panel D and concave in panel E. Note that the sample shown in panel E is atypical in the sense that the concave curvature persists after the end of drying. Also, the curvature is much stronger than usual. This sample has been chosen for the purpose of demonstration. The white bar in panel E denotes a cut through the sample. The stresses displayed in Figures 3, 5, and 6 are taken along such cuts through the center of the sample.

Generally speaking, this instrument has confirmed the conventional picture of drying. In particular, one often finds a front of tensile stress, propagating from the edge of the film toward the center. The stress front is the consequence of edge-in drying. However, we have also encountered *dilational* stress under a variety of conditions. We elaborate on these conditions and propose a mechanism explaining it.

Experimental Section

Materials and Experimental Protocol. The results reported here were obtained on a coatings formulation ($T_g \sim 18$ °C). The material was prepared by miniemulsion polymerization.[21,22] The polymer phase was a 1:1 copolymer of butyl acrylate (BA) and methyl methacrylate (MMA). Acrylic acid had been added to the recipe at a weight fraction of 1% for the purpose electrosteric stabilization. The emulsifier was Dowfax 2A1, which is an anionic sulfonate. The particle size was in the region of 100 nm. The initial solids content of the master batch was 49 wt %. In order to adjust the solids content, the master batch was diluted with Milli-Q water down to solids contents of 38, 28, and 20 wt %.

Drops with a volume of 150 μL were deposited on the membrane and spread to a diameter of about 2.5 cm. The wet thickness was about 300 μm. Apart from the convexly shaped rim, the surface of the sample is flat after spreading. The experiments occur on *films* rather than droplets. "Time" in the following always refers to time after deposition. All experiments were performed in stagnant air. Temperature and humidity were 25 °C and 45% rh, respectively.

Stress Mapping. The instrument used for the determination of stress maps is described in detail in ref 20. The film of interest is deposited on a flexible, partially reflective membrane, which is stretched across a rigid frame (Figure 1A). The membrane warps under the influence of the drying-induced surface stress. The deformation is quantified by imaging a regular object (a grid) across the back of the membrane. The membrane serves as a distorted mirror.

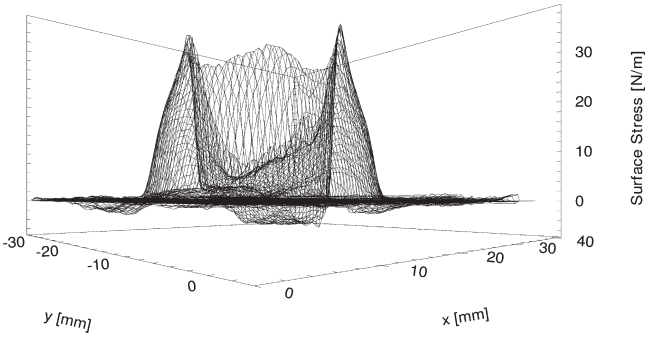

Figure 2. A typical stress map showing dilational stress in the center of the sample.

For demonstration of upward and downward bending (Figure 1B−E), we have taken images of a grid reflected from the back of the membrane after the membrane was removed from its frame. In the case shown in Figure 1E, the dilational stress had persisted after drying was complete. The back of the membrane therefore acts as magnifying mirror. Nota bene: a concave shape *after* the end of drying is untypical. We chose this sample for the purpose of demonstration. Most samples only show transient dilational stress. Also, the imaging conditions (the distance of the grid from the mirror, in particular) have been chosen to produce a convincing photograph. When the membrane is stretched across the frame, the image distortion is much smaller. In fact, the distortion is *required* to be small for quantitative analysis.[20]

Via automated image analysis we create a map of vertical displacement of the membrane, $u_z(x,y)$. Assuming that the stress is the same along x and y (in-plane isotropy) and, further, that the bending stiffness of the membrane is negligible, one can convert $u_z(x,y)$ to a surface stress $\sigma_f(x,y)$ (in units of N/m) via the relation[20]

$$\sigma_f(x,y) = \frac{2\Gamma}{d_m} u_z(x,y) \quad (1)$$

Here, Γ is the lateral tension of the membrane (in units of N/m) and d_m is the membrane thickness. Γ was calibrated by placing known weights onto the membrane.[20] Γ and d_m were around 70 N/m and 12 μm in the experiments reported here. Figure 2 shows a typical stress map. Positive stress here is tensile stress. While the stress is tensile at the rim of the sample, it is negative (dilational) in the center.

In principle, one might convert the surface stress, σ_f, to an average bulk stress, $\langle\sigma\rangle$, by dividing by the film thickness. However, since the stress distribution along the vertical may very well be heterogeneous, such a conversion is potentially misleading and was therefore avoided.

Results

In order to compare the stress profiles at different drying times, we display the surface stress along a cut through the center of the sample (cf. the white bar in Figure 1E) in Figure 3. The top panel shows data obtained on a sample with an initial solids content of 49%. The (tensile) stress first develops at the edge because of edge-in drying. With continued solidification, the stress front propagates toward the center, until the entire sample is under stress. For the sample with an initial solids content of 38%, the behavior is characteristically different (bottom panel in Figure 3). As before, there is a maximum in tensile stress at the rim shortly after deposition. Contrasting to the data shown at the top, the stress in the center now is negative at intermediate drying times. Only at the end of drying does tensile stress supersede this effect. Visual observations show that buckles develop at those places, where the stress is dilational (Figure 4).

(21) Asua, J. M. *Prog. Polym. Sci.* **2002**, *27*, 1283.
(22) Antonietti, M.; Landfester, K. *Prog. Polym. Sci.* **2002**, *27*, 689.

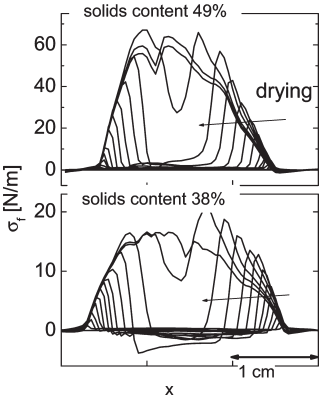

Figure 3. Stress profiles along a section through the film (cf. the white bar in Figure 1E) at different times. The dispersions with high solids content (top) only experiences tensile stress. The diluted dispersion (solids content of 38%) does show dilational stress.

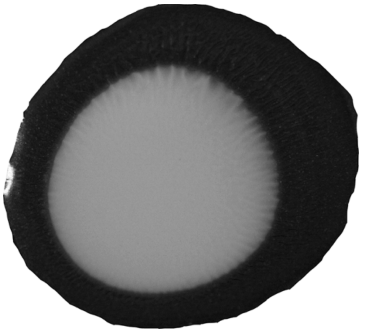

Figure 4. Photograph taken after 80 min of drying (initial solids content of 28%). Buckles appear ahead of the drying front. The buckles stay. They are not visible in the black areas because the film has turned transparent.

Figure 5 shows the stress evolution for all solids contents as a contour plot. The vertical and the horizontal axis are time and position, respectively. The absolute values are encoded in a gray scale, where negative (dilational) stress is hatched. Again, one always observes a front of tensile stress originating at the edge. For low solids contents, one also finds dilational stress. For the sample with the highest dilution (20% solids content), the dilational stress persists after the end of drying. In all other cases, tensile stress eventually dominates. The dilational stress is both localized and transient. In Figure 6, we compare the stress between the different dispersions. This time was chosen as about 2/3 of the total drying time, where the latter time is the time when the sample turns transparent. The respective times are indicated as white bars in Figure 5.

The most important consequence of dilational stress in terms of practical application is buckling. The samples investigated here showed both buckling and cracking. Cracks in Figure 7 have sharp edges (full circles) while buckles appear a bit more diffuse (dotted circles). The distinction between buckles and cracks is most clear when observing the samples while it dries. The buckles appear ahead of the drying front, while the cracks are formed after the samples have turned clear (Figure 4). We observe cracks in these films even though we work at $T > T_g$ because the films are thicker than usual. One may form crack-free films from this material with a dry thickness below 30 μm.

Discussion

Figure 8 illustrates the mechanism which we believe to be origin of dilational stress. The stress occurs at the time when all particles have solidified and the flow of material from the centers toward the drying front stops. Until this time, the liquid has exerted a viscous drag onto the particle network. In order to achieve mechanical equilibrium, the network forms in such a way that it compensates for the drag forces by an internal elastic stress. The network may be viewed as a spring, which is formed while there is an external force. Once the flow stops, the external stress disappears. The spring (the network) now expands and bends the substrate downward. For instance, one may depict the particles as small ellipsoids in the compressed state and as spheres once the viscous drag has ceased. Actually, the deformation will presumably be confined to an area close to the contact between the particles because the stress is large there. It is implausible for a sphere slightly above T_g to be squeezed into ellipsoids. Local elastic deformations at the point of contact, on the contrary, are reasonable. From a contact mechanics point of view, it is more likely that the points of contact are strained by the viscous drag and assume a less strained state once the flow has stopped. Whether and how the dilational stress relaxes depend on the details. It may relax via a buckling of the entire film. It may also be superseded by further compaction. Evidently, it may also relax by flow on the local scale or not relax at all. According to the model, dilational stress should occur coincidently to the dynamic arrest of the particles. While we cannot correlate dilational stress with dynamic arrest for the samples discussed here, we did find in earlier experiments[23] such a correlation for samples containing either titania of clay filled acrylate particles. The correlation was established based on photon correlation spectroscopy in conjunction with membrane bending. The occurrence of dilational stress coincided with the appearance of a strong static component in the autocorrelation function. This static component is caused by an immobile network of particles. These results suggest that dilational stress indeed appears at the time, where the particles start to form a network.

In the following, we make the above considerations more quantitative. Following the coordinates shown in Figure 8, with $x = 0$ defined as being the edge of the film, the pressure in the compacted region of the film is assumed to follow Darcy's law[24]

$$u = \frac{-k_p \mathrm{d}p}{\mu \ \mathrm{d}x} \tag{2}$$

with u the fluid velocity in the horizontal direction, k_p the bed permeability, μ the solvent viscosity, and $\mathrm{d}p/\mathrm{d}x$ the pressure gradient. A solvent mass balance, subject to an evaporation rate of $\dot{E}$ per unit length and film height h, results in

$$\frac{\mathrm{d}}{\mathrm{d}x}(hu) = -\dot{E} \tag{3}$$

Combining eqs 2 and 3 results in a second-order differential equation for the pressure in the compacted region of the film.

$$\frac{\mathrm{d}}{\mathrm{d}x}\left(h\frac{\mathrm{d}p}{\mathrm{d}x}\right) = \frac{\mu\dot{E}}{k_p} \tag{4}$$

Solving eq 4, subject to boundary conditions of zero velocity ($\mathrm{d}p/\mathrm{d}x = 0$) at $x = 0$ and a zero pressure at the fluid solid transition, $x = x_f$ results in the fluid pressure as

$$p = \frac{\mu\dot{E}}{2k_p h}(x^2 - {x_f}^2) \tag{5}$$

(23) von der Ehe, K. Detection of Stress During the Drying Process of Polymer Dispersions. PhD Thesis, Clausthal University of Technology, 2008.
(24) Deen, W. *Analysis of Transport Phenomena*; Oxford University Press: New York, 1998.

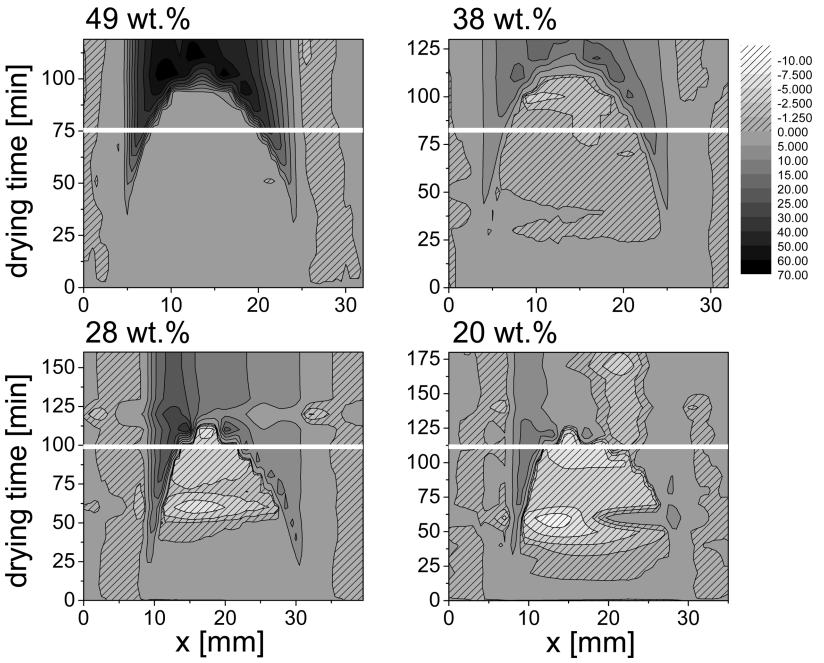

Figure 5. Stress evolutions for dispersions with solids contents of 49, 38, 28, and 20 wt %. The x-axis and the y-axis are position and drying time, respectively. Stress values are encoded in gray. Negative (dilational) stress is hatched. White bars denote the times corresponding to the data shown in Figure 5.

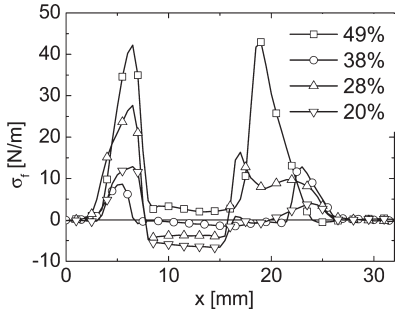

Figure 6. Comparison of stress profiles from different initial solids contents at a time equivalent to 2/3 of the total drying time (that is, the time until the films turn transparent).

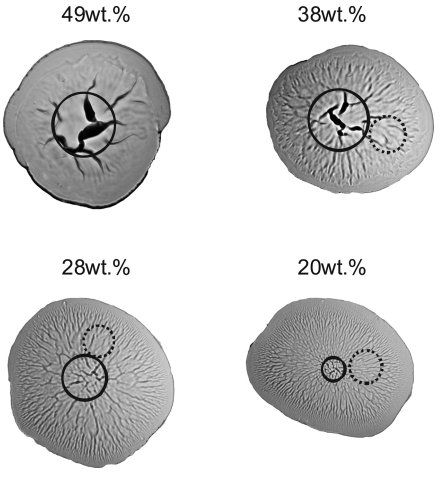

Figure 7. Photographs taken after the end of drying. The cracks (solid circles) are produced late in the drying process. The buckles (dotted circles), on the contrary, appear *ahead* of the drying front.

It has been assumed that the film height, h, is constant. This is obviously a simplification but allows simple expressions for the pressure distribution to be obtained. If the constant height assumption is relaxed, the pressure distribution is calculated to be $p = (\mu\dot{E}/k_p)\int x_f^x(x/h)\,dx$. The pressure is negative and results in a compression in the film. Vertically, this is the stress that results in capillary deformation. Horizontally there must also be a compression and we can estimate the average pressure, again assuming constant height as

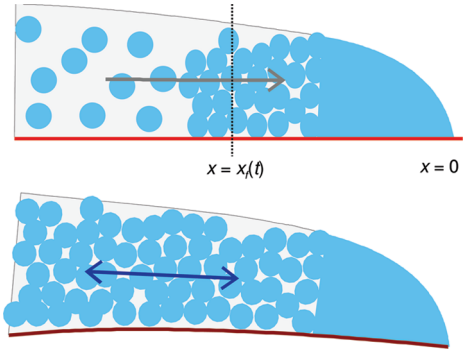

Figure 8. Sketch of the postulated mechanism leading to dilational stress. At the time when the elastically coupled network of spheres forms, there is a viscous drag onto the network, exerted by the flow of liquid toward the drying front. The network is under internal stress, thereby compensating for the viscous stress. Internal stress has been depicted as a deformation of the spheres in the sketch (spheres turn into ellipsoids). The deformation pattern presumably is not as simple as in the sketch. After cessation of flow, the network expands, thereby producing a lateral expansion and downward bending of the substrate.

$$\bar{p} = \frac{1}{x_f}\int_0^{x_f} p\,dx = \frac{-\mu\dot{E}x_f^2}{3k_p h} \qquad (6)$$

Note that the quantity determined in experiment is a surface stress. In order to convert from bulk stress, $\bar{p}$, to surface stress, σ, one needs to multiply by the film thickness, h. h is the film thickness at the time of solidification, which is slightly higher than

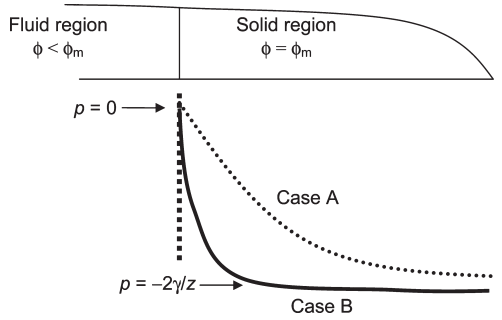

Figure 9. Sketch of pressure profiles in the solidified region of the film. Case A corresponds to eq 5 and assumes that the pressure is always lower in magnitude than the capillary pressure. Case B corresponds to the case where the film reaches its maximum capillary pressure quickly and the pressure is then spatially constant.

the dry thickness. Following eq 6, the model therefore predicts that there is no explicit dependence of the surface stress on the film thickness. Once the film solidifies, everywhere the horizontal drying stops. At the instant before solidification occurs the particle front has almost reached the center of the film, and hence $x_f = x_c$ where x_c is the radius of the sample. The governing equation for the pressure distribution remains the same (eq 5); however, the boundary conditions become zero pressure gradient at the film edge and center ($u = 0$ when $x = 0$ and x_c). Only the trivial solution ($p \equiv 0$) satisfies the boundary conditions. This signifies that the picture of a flow of solvent through the particle no longer applies, and the physical situation is of a stagnant fluid with a spatially constant pressure, which increases with time. The magnitude of the pressure originally is difficult to estimate but if taken as zero, which will be the pressure in the center just at the point of compaction, then a constrained film will experience a dilational stress equal to the stress imposed on the film by the horizontal drying. Hence, a dilational stress of magnitude $\mu \dot{E} x_c^2/3k_p h$ will be observed.

The parameter k_p, the "bed permeability", depends on the details of the geometry and is hard to predict. The discussion above can be further simplified if a different view is taken of the stress distribution. According to eq 6, the pressure is a monotonically decreasing function with the largest magnitude at the edge. However, there is a maximum magnitude of the pressure that can be supported: the capillary pressure. The different pressure distributions are sketched in Figure 9, and if the pressure is assumed to be at its maximum value, then the average pressure $\overline{p}$ can be estimated as the capillary pressure $2\gamma/z$, where γ is the air−water surface tension and z is the radius of the curvature of the menisci. z is about one-tenth of the particle radius.

This estimate says that the observed pressure should be of the same order of magnitude as the capillary pressure. The same argument has been made before[25] and has actually been used to rescale the stress. One defines a normalized stress, which is the ratio of the bulk stress and $2\gamma/z$.[26] The stress found in film-drying experiments rarely exceeds $2\gamma/z$ and is of that order of magnitude for sufficiently hard spheres. This rule of thumb holds for the dilational stress as well. Using a sphere diameter of around 100 nm, a surface tension of 35 mN/m (for water containing surfactant), a thickness of the film $h \sim 60-150\ \mu$m, and a surface stress of around $\sigma_f \sim 30-70$ N/m (see Figure 5), we arrive at a normalized stress of $<\sigma>/(2\gamma/z) = \sigma_f/h/(2\gamma/z) \sim 0.07$. This value

(25) Tirumkudulu, M. S.; Russel, W. B. *Langmuir* **2005**, *21*, 4938–4948.
(26) The authors of ref 25 use the particle radius, r, instead of z.

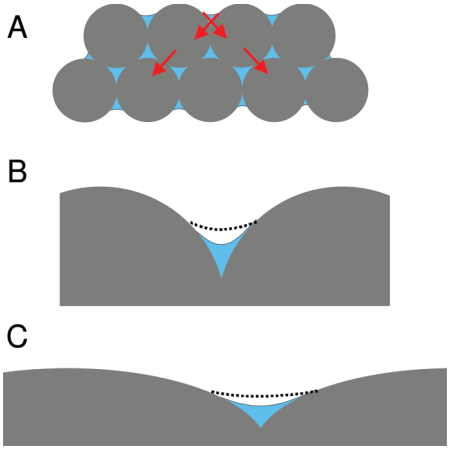

Figure 10. A meniscus exerts a vertical force onto the topmost layer of spheres (A). Upon vertical shrinkage water moves upward and thereby decreases the area of the air−water interface at the meniscus (B). If the network of spheres behaves like an elastic body with positive Poisson's number, the network might, in principle, expand laterally. However, such a motion would *increase* the area of the liquid−vapor interface, rather than decreasing it (C). If lateral expansion is coupled to an increase of the surface energy, it cannot be driven by surface energy because surface energy always should be decreased.

is in the expected range. The above estimates assume perfect recoil of the compacted bed.

Conclusions

Employing an apparatus to measure spatiotemporal patterns of stress, we investigated the mechanisms leading to dilational lateral stress during the drying of latex dispersions. Dilational stress in most cases is a transient phenomenon. The occurrence of dilational stress correlates with the solids content. We attribute dilational stress to an internal stress of the particle network, which forms while there is a drag force exerted onto the network by the lateral flow of liquid. Once the flow stops, the network relaxes and thereby expands laterally. The phenomenon should be present in all cases where there, first, is lateral flow of liquid during drying, and second, the particles display some elasticity at that time of drying. Both conditions are frequently met.

Acknowledgment. This work was funded by the EU under Contract IP 011844-2 (Napoleon). We thank Raquel Rodriguez and Maria Barandarian (University of the Basque Country, San Sebastian) for preparing the latex.

Appendix. On Dilational Stress Created by Capillary Pressure

In the literature, there is a claim that dilational stress may originate from capillary pressure alone.[27] One of us has previously argued along the same line.[19] Reanalyzing the situation and considering the boundary conditions in detail, we come to the conclusion that this explanation is inapplicable here.

Consider the geometry displayed in Figure 10A. Clearly, there is a vertical force onto the top layer of the spheres, pushing them downward. In principle, the network of spheres may be viewed as a viscoelastic medium with positive Poisson′s number. Upon

(27) Pekurovsky, L. A.; Scriven, L. E. On Capillary Forces and Stress in Drying Latex Coating. In *Film Formation in Coatings - Mechanisms, Properties, and Morphology*; Provder, T., Urban, M. W., Eds.; American Chemical Society: Washington, DC, 2001; Vol. *790*, pp 27−40.

vertical pressure, they might, in principle, expand laterally. References 19 and 25 follow this line of argument.

However, this argument neglects the fact that the motion of the spheres and the motion of the liquid are coupled. We believe that the situation becomes more transparent by considering energies (rather than forces). All capillary forces are ultimately driven by a reduction in interfacial energy, which amounts to a reduction of the area of the air−water interface. Consider an entirely vertical motion of the spheres, first (Figure 10B). As the spheres move down, the water moves up, fills the interstitial space at the air−water interface, and thereby reduces the surface area (dotted line in Figure 10B). If, however, the network expands laterally, this will *increase* the surface area (Figure 10C). Such a type of deformation cannot be driven by capillary forces because what ultimately drives capillarity is surface energy.